FINITE ELEMENT BASED MICRO-MECHANICS MODELING OF TEXTILE COMPOSITES *

E.H. Glaessgen† and O.H. Griffin, Jr.††
Department of Engineering Science and Mechanics
Virginia Polytechnic Institute and State University
Blacksburg, VA 24061

SUMMARY

Textile composites have the advantage over laminated composites of a significantly greater damage tolerance and resistance to delamination. Currently, a disadvantage of textile composites is the inability to examine the details of the internal response of these materials under load. Traditional approaches to the study of textile based composite materials neglect many of the geometric details that affect the performance of the material.

The present three dimensional analysis, based on the representative volume element (RVE) of a plain weave, allows prediction of the internal details of displacement, strain, stress, and failure quantities. Through this analysis, the effect of geometric and material parameters on the aforementioned quantities are studied.

INTRODUCTION

Textile based composite materials have received considerable attention in the literature in recent years [1,2]. These traditional approaches to the study of textiles are typically an extension of proven techniques for the study of laminated materials. They tend to be based on strength of materials and classical lamination theory (CLT), a homogenized finite element approach that uses classical micromechanics or CLT as a basis for material properties, or a spar in a matrix approach [3]. The result is a lack of ability to determine details of the internal response of these materials under load. A macro finite element approach was developed by Whitcomb [4] and Woo and Whitcomb [5] and is a compromise between the previously mentioned models and the type of detailed finite element models developed for the present study. Although the analysis by Whitcomb shows some details of the load distribution within the composite, it may neglect some of the geometric details that affect the performance of the material. Techniques employing conventional finite elements have also been reported [6,7,8]. These have been developed for woven composites under mechanical loads and provide varying degrees of accuracy and details of results.

* Work performed under grant NAG-1-343 at Virginia Polytechnic Institute and State University
† Graduate Research Assistant
†† Professor and Associate Dean

The present finite element based technique allows the interrogation of the internal response of textiles. This approach greatly reduces the geometric simplifications required for modeling, since the finite element models are taken directly from either the Textile Geometry Model (TGM) [9] or from micrographs of manufactured materials. Although originally developed for the analysis of textiles under mechanical loads [6], this technique is easily extended to include response to thermal loading. The present analysis, based on the representative volume element (RVE) of a textile composite, allows prediction of the load, mode, and location of failure initiation within the RVE. Through these models, not only is gross characterization possible, but internal details of displacement, strain, stress, and failure parameters can be studied. Specifically, this discussion focuses on the analysis of a plain weave textile composite. Both mechanical and thermal loading is considered.

GEOMETRIES STUDIED

Although it is desirable to avoid more geometric simplifications than necessary, certain simplifications are unavoidable. Sectioning of manufactured woven textile composites shows that material variances exist throughout the textile. Accounting for the differences between RVEs in a given architecture must be treated as a statistical problem and is beyond the scope of this paper, instead, a "typical" geometry is studied. The yarn center line is assumed to be a smooth (order O2) b-spline while the cross-section is an O2 b-spline of an elliptical shape. The RVE is assumed to repeat both its geometr and response throughout the entire material. Details of the construction of the finite element model are given in an upcoming section.

In the present study, the geometry is determined by sampling points on the yarn centerline and cro: sectional perimeter of a fabricated material [10]. Details of the RVE size and yarn dimensions are given . Table 1. As shown in Figure 1, the geometric rendering of the RVE, the x and z directions are the in-plan

Table 1: Model Geometry

RVE size (in)	a / b, axial yarn (in/in)	a / b, transverse yarn (in/in)
0.275 x 0.050 x 0.1960	0.0787 / 0.0098	0.0866 / 0.00866

directions, while y is the out-of-plane direction.

MATERIAL SELECTION

One unfortunate limitation of the finite element method is that the geometry and material properties must be selected a-priori. As with the geometric parameters, representative values of the material properties commonly found in textile composites are used. The values have been chosen to represent

typical glass/epoxy and carbon/epoxy materials. The material properties are given in Table 2.

Table 2: Material Properties

Material Properties	Epoxy	Glass / Epoxy	Carbon / Epoxy
E_x (E6 psi)	0.5	5.5	23.0
E_y (E6 psi)	0.5	1.43	1.58
E_z (E6 psi)	0.5	1.43	1.58
G_{xy} (E6 psi)	0.1875	0.59	1.00
G_{xz} (E6 psi)	0.1875	0.59	1.00
G_{yz} (E6 psi)	0.1875	0.55	0.60
υ_{xy}	0.33	0.27	0.27
υ_{xz}	0.33	0.27	0.27
υ_{yz}	0.33	0.30	0.30
α_x (E-6 in/in F)	25.0	4.83	0.010
α_y (E-6 in/in F)	25.0	19.6	11.50
α_z (E-6 in/in F)	25.0	19.6	11.50

SOLID MODEL

The response of a fiber reinforced material is dependent on the type of reinforcement, constituent material properties, and physical location and orientation of the reinforcement. In the case of a textile reinforced composite, quantification of the geometrical structure of the of the reinforcement is rather complex. Thus, the first step in a detailed modeling approach is the development of methodologies for predicting the positions and orientation of the yarns contained in the RVE. The details of the Textile Geometry Model and its use in predicting the textile geometry are given in Pastore, et.al. [9].

Once the yarn cross section and spline data are obtained from the TGM, they are directly converted to a format suitable for use in SDRC I-DEAS 6.1, the solid modeling and mesh generation package used for this study. First, the cross section of the yarn is input as a series of discrete points on the yarn surface. These points are fit to a b-spline representing the yarn perimeter. Second, the yarn centerline points are input and fit to a b-spline in a similar manner. The I-DEAS skin group for the yarns is developed by first creating a profile from the b-spline fit yarn cross section. The profile is dragged along the sectional spline to develop the yarn skin group. The logical flow for this process is illustrated in Figure 1c.

The solid modeling routines in I-DEAS are used to translate the yarn skin group to a yarn solid object. Creation of additional yarns proceeds in one of two ways. If an additional yarn is merely a translated or rotated version of the original, the appropriate I-DEAS commands are executed to perform the translation/rotation operation. If the yarn is a unique (not a translated or rotated version of the previous

yarn), the original yarn creation process is repeated beginning with the surface and/or spline points. Once created, all of the yarn solid objects are oriented in three-dimensional space to correspond to their locations within the textile geometry model (TGM), as shown in Figure 1d.

The outer boundaries of the representative volume element (RVE) are represented as a hexahedral shaped solid object oriented with its centroid at the centroid of the RVE. The boolean capabilities within I-DEAS are used to subtract the yarns from the outer block. The object that remains corresponds to the surrounding matrix contained within the RVE as shown in Figure 1a and 1b.

Once the RVE solid containing the details of the interior boundaries of the textile has been developed, the mesh areas and mesh volumes are created. The volume having the same boundaries as the original volume is considered the matrix finite element volume, while the yarn volumes become yarn finite element volumes.

FINITE ELEMENT MODEL

Because of their three-dimensional structure, textiles tend to be computationally expensive to model with finite elements. Thus, it is desirable to model the RVE with as few elements as required for convergence. This leads to consideration of hexahedral elements, in particular to the quadratic hexahedra Models composed of this element tend to converge quickly for a given number of degrees of freedom. However, current mesh generators can use this element only in conjunction with five and six faced volumes. Since the RVE may contain dozens or even hundreds of faces, the process of further subdividin the original single volume of the RVE into an appropriate number of five and six sided subvolumes becomes prohibitively time consuming. Conversely, a mesh composed of quadratic tetrahedral elements can be used to discretize the complete matrix volume into finite elements. The yarn volumes are also discretized as complete volumes. The main disadvantage of tetrahedra-based meshes is the size of the resulting finite element models. Tetrahedra-based meshes are generally much larger than comparable hexahedra-based meshes.

Convergence of a finite element mesh can be determined through several methods. The method used here is perhaps the most straightforward albeit most computationally expensive method. Here, the domain is meshed with an ever increasing level of refinement. If two consecutive refinements yield results that differ by a sufficiently small amount, the former mesh is said to be converged. Typically, a few percent is used as a criterion.

Choice of proper discretization for volumes as complicated as those found in textiles leads to a trade-off between mesh convergence and model size. A typical global element size is approximately 1/20 of the model characteristic dimension, while local refinements are made to ensure convergence in known regions of high stress gradient. Once the finite element discretization of both the matrix volumes and the yarn volumes has been completed and checked for element distortion, a concern considering the complex shape of the mesh volumes, the element coordinate systems of the yarn elements are aligned with the b-spline defining the orientation of the yarn volume. This alignment insures that the yarn finite elements will behave as subdomains within a homogeneous piecewise transversely isotropic material with the properties given in Table 2. Both materials were modeled with 10-node tetrahedron (ABAQUS C3D10) elements.

FINITE ELEMENT MODEL - THERMAL LOADING

In addition to mechanical loading (to be discussed later), complete analysis of any structural material requires that thermal loading be considered. Textile composites may be subjected to thermal loads both during the curing process and during in-service temperature changes.

A uniform temperature change is considered as it is a fundamental case when considering the structural behavior of a material under thermal loading. Typically, textile preforms are layered and are many RVEs wide, thus it is appropriate to consider that a randomly selected RVE may be subjected to virtually any degree of constraint. This becomes important when accounting for the relative position of a RVE within a textile preform. To bound the limits of constraint, five boundary conditions are considered. These are: 1) periodic, 2) out-of-plane symmetry, 3) out-of-plane free, 4) in-plane symmetry, and 5) in-plane free boundary conditions.

The first of these boundary conditions, periodic, represents the upper bound of constraint, a RVE far from any boundary. To simulate this situation, the opposing faces are restrained with multi-point constraints (MPC) to remain uniformly straight and parallel to one another. The second, out-of-plane symmetry, is an intermediate case similar to the behavior of a two layer un-nested textile. Out-of-plane free boundary conditions are representative of the least constrained RVE, that is, a composite that is one RVE thick. While the out-of-plane symmetry case has one free face, the out-of-plane free case has both top and bottom surfaces free to deform from their original planar state.

Of the two in-plane variations, the in-plane symmetry case is an intermediate degree of constraint representing a narrow composite two RVEs wide. The final case, in-plane free, is the lower bound of restraint, a composite one RVE wide. In this last case, the material is assumed to have two edges that are allowed to deform freely.

In all cases, a uniform temperature change of one degree Fahrenheit is applied to each element within the finite element model. Although this represents the steady state loading condition, geometric complexities and material dissimilarities are sufficient to induce the complex behavior shown in the results portion of this paper.

The results that follow are based upon the finite element models discussed in the preceding section. The results are divided into two main sections: 1) displacements, and 2) strain energy density. The later quantity is discussed because it is the basis of many energy based failure criteria and also provides a useful scalar quantity for visualization independent of material coordinate system.

Note that familiar terms are used in describing the geometry of the RVE. For example, "lower" and "upper" refer to the surface having most negative y coordinate (y= -0.025 in.) and the most positive y coordinate (y= +0.025 in.), respectively. Also, numbers in parenthesis correspond to a specific detail on the figure being discussed.

The models have been checked for convergence, and for the idealized geometries considered, are

converged to within a few percent. However, in the figures that follow, it may be more beneficial to consider the qualitative nature of the isosurfaces than it is to compare exact numbers represented by the isosurfaces.

DISPLACEMENT RESULTS - PERIODIC BOUNDARY CONDITIONS

The isosurfaces illustrated in Figure 2a represent the computed internal axial displacements of a well restrained region within plain weave textile composite under a uniform temperature change. As prescribed by the boundary conditions, the exterior boundaries remain planar and parallel. Displacements within this RVE are, as expected, the most uniform. Although not planar, every point on the surface (1) is 12.5% of the maximum value. It can be thought of as representing the average axial strain in that part of the model. Thus, the axial yarn is seen to strain more than the transverse yarn that is just above it in the RVE. Further, recalling elementary elasticity, the angular change in the displacement isosurface (1) can be compared directly to a local shear strain. The sharper the angle, the greater the shear strain. This "shear strain" is seen in both the x-y and x-z planes.

Figure 2b represents the out-of-plane deformation associated with periodic boundary conditions. Note that the maximum value of out-of-plane displacement is 83% larger than the corresponding in-plane displacement for these boundary conditions. This occurs for two reasons: 1) the coefficient of thermal expansion (CTE) of the yarn's transverse direction is much greater than the CTE in the yarn axial direction, and 2) the in-plane stiffness of the axial and transverse yarns restrains the in-plane deformation.

As with the in-plane deformation for this fully restrained case, the top and bottom boundaries are forced to remain straight and parallel from the applied boundary conditions. However, internally, the deformations are as shown (1).

Figure 2c is the baseline of transverse displacement (fully constrained) for the RVE models. Again, the outer boundaries are allowed to deform in a planar fashion only. Although the temperature change is uniform in the x and z directions, as indicated in Table1, the RVE geometry is not uniform. Thus it is reasonable to expect that the internal deformation behavior is not uniform in the two in-plane directions.

DISPLACEMENT RESULTS - OUT-OF-PLANE BOUNDARY CONDITIONS

When the upper surface of the RVE is released to deform out-of-plane, the reduced constraint results in the axial deformation shown in Figure 3a. This case is representative of a layer of a two layer un-nested composite and provides an intermediate condition to the fully restrained case shown in Figures 2, and the unconstrained case that will be seen as Figures 4. Note here that the lower portion of isosurface (1) shows a similar deformation as the lower portion of isosurface (1) in Figure 2a, whereas the free condition on the top surface localizes the axial deformation to the region between the transverse yarns. As before, the local strains associated with isosurface (1) can be visualized as the ratio of the value of displacement

represented by the isosurface (12.5% of $U_{x,max}$) to the distance from the isosurface to the left side boundary. Thus, a disproportionate percentage of the axial deformation occurs in the most axially compliant region of the RVE (2).

Out-of-plane deformations, Figure 3b, are "dish" shaped. Now, the restraint on out-of-plane deformation is relaxed, and the upper surface is allowed to deform freely. Note the isosurface shown is at 50% (1), while the bottom surface is the fixed, or 0%, surface. This surface is concave, and the maximum displacement occurs above the point of maximum concavity. For clarity, isosurfaces other than the one at 50% have been omitted from the plot; however, it is important to note that the maximum value of displacement occurs along a surface that is a function of the local weave geometry.

By further decreasing the constraint on the model to allow for both top and bottom surfaces to freely deform, a situation as shown in Figure 3c results. In the regions of maximum constraint (those regions near the yarns), the axial displacement isosurfaces (1) are similar to those in the fully restrained case (Figure 2a). However, differences are greatest in the more compliant regions away from the yarns. Here, the angular change in isosurface and resulting shear strains are reduced because of the absence of the planar constraint.

An interesting artifact in Figure 3d is (1), the isosurface of 50% of the maximum out-of-plane displacement. Because of the angle from which this image was taken, it appears that considerable out-of-plane deformation occurs at (1), while little occurs at (2). Actually, because of the anti-symmetric geometry, the two regions of the displacement are anti-symmetric. Because of the absence of in-plane constraint, the maximum deformation is 47% larger than for a similar layer embedded within the composite (Figure 2b). Thus, it is possible to conclude that there is a non-uniform displacement gradient not only within the individual RVEs (Figure 3d), but among the several RVEs through the thickness of a typical textile composite, and that it is a function of their position from the center-line of the composite.

DISPLACEMENT RESULTS - IN-PLANE BOUNDARY CONDITIONS

To simulate a free edge, the front boundary of the RVE has been un-constrained in Figure 4a to allow free deformation. Note that the axial deformation along the back, or constrained, surface (1) is similar to the axial deformation in the same region for the fully constrained case. However, a very different condition exists at the free edge. A disproportionately large percentage of the total axial deformation occurs near the compliant center of the front edge (2). Further, increased shear strains develop. For example, the x-y component of shear strain, shown as an angular change in the isosurface, is prominent along the front edge (3).

Figure 4b illustrates the transverse deformation, in particular, the transverse deformation along the free edge. Nominally, only slightly more than 25% of the total deformation in the RVE occurs in the back half (1) of the RVE. Also, the greatest transverse deformation occurs near the center of the RVE. This is the least constrained (transverse) region of the model both because of the domination of the region by axial yarns and by its distance from the stiffening effects of the restraints along the transverse edges (2).

When both the front and back edges of the RVE are released, simulating a composite one RVE wide, the axial deformation is as shown in Figure 4c. The internal deformation is redistributed such that the axial strain varies greatly with position from the x-axis (1). Further, the center of the RVE, the matrix dominated region, is found to be in a state of near constant displacement (2).

Corresponding transverse displacements are shown in Figure 4d. Similar to the transverse displacements shown in Figure 4b, the compliant region away from the front/back edge boundary conditions and the transverse yarns, has the greatest transverse displacement. The combined constraining effect of planar edges and transverse yarns is similar to the thermal expansion case for a plate with cantilevered edges. The center is allowed to displace from the nominal centerline of the edge, however, the displacement is not as large as if the edges were allowed to rotate freely

The largest transverse displacement is 50% larger than for the case of one free edge and over 400% larger than for the fully constrained case. A comparison can be made with the free edge case for laminated composites where the edge displacements are seen to vary as a function of through thickness (y) coordinate along the edge. In contrast to the laminate, the transverse displacements for the textile are also greatly dependent on axial coordinate (1).

STRAIN ENERGY DENSITY RESULTS

Strain energy density (SED) results for the case of periodic boundary conditions are shown in Figure 5a. The SED distributions in this model correspond to the displacement distributions shown in Figures 2 discussed previously. The left and right hand regions shown in (1) are similar. In the figure, the two regions of the isosurface are anti-symmetric as a function of the yarn geometry.

Note that the yarns contain much of the SED in the model (1), while the largest values of SED are found in the regions of the matrix immediately above and below the axial/transverse yarn crossovers (2). Because this architecture is not quite balanced, the maximum values occur at the alternate corners on the top and bottom of the model (3). Checking the stresses and strains in the several regions of interest indicates that a matrix failure primarily due to through-thickness tension at region (3) is the likely first failure.

The centerline paths of the axial yarns are not fully antisymmetric for this geometry. An important result of this geometric artifact is that the distance from the axial yarn outer surface to the horizontal boundary of the RVE is different for adjacent pairs of interstices. Thus, of the eight corner locations in the RVE, there are two pair of four distinct values of SED. A typical pair is shown in (4).

Since SED is a scalar product of strain and stress components in the model, it is always zero or positive for conservative systems. As shown in Figure 5a, it is greater than zero for all locations within the model and reaches a maximum of 6.68E-4 in-lb/in^3 in regions (3).

When the out-of-plane restraints are removed from the top and bottom surfaces, the strain energy distribution is shown in Figure 5b. This figure corresponds to the displacements shown in Figures 3 that have been discussed previously. Large values of SED are found in the corners of the matrix similar to the

fully restrained case (1). However, the largest values of SED in the model are found in alternate inboard locations (2) and (3) and result primarily from the combined effect of through-thickness and axial tension. Thus, while the material exhibiting the maximum SED has not changed, the location has been altered significantly.

When the in-plane restraints are removed from the front and back surfaces, the strain energy distribution is similar to that in Figure 5c and corresponds to the displacements in Figures 4. The largest values of SED are very localized such that the interior cusp regions of the transverse yarns contain all the SED above 30% of the maximum (1). The maximum value of SED is increased by 165% over the fully restrained case. Now, the mode has changed to axial tension in the transverse yarns as determined in the local coordinate system.

In contrast to the mode and location shown in Figure 5a for a carbon/epoxy system, if the material parameters are changed to simulate glass/epoxy, strain energy density values such as those in Figure 5d result. The yarns contain all of the SED above 40% of the maximum value. However, in the glass/epoxy material system, the thermal and mechanical mismatches are not as severe as with carbon/epoxy. The largest values of SED are found near the centerline of the yarns (2) and are primarily the result of axial loads in the local coordinate systems.

FINITE ELEMENT MODEL - MECHANICAL LOADING

A uniform axial extension is the fundamental case when studying the behavior of a material under mechanical loading and will be discussed here. For this load case, the positive x-face (Figure 1) is displaced uniformly by a displacement producing a nominal strain of 1000 micro-strain (0.00275 in. applied axial displacement through 0.275 in.), the negative x-face is restrained from displacement in the axial direction, and the other faces are subjected to restraints simulating extremes of position within the overall structure. As with the case of thermal loading, the following limiting cases are considered: 1) periodic, 2) out-of-plane symmetry, 3) out-of-plane free, 4) in-plane symmetry, and 5) in-plane free boundary conditions.

DISPLACEMENT RESULTS - PERIODIC BOUNDARY CONDITIONS

The isosurfaces shown in Figure 6a represent the computed internal axial displacement of a well constrained region within the plain weave textile composite under uniform axial extension. As with Figure 2a (uniform temperature change), the exterior boundaries remain planar and parallel. Unlike the case of uniform temperature change, the isosurfaces are representative of a near uniform axial displacement gradient (1). Since the axial yarns dominate the axial stiffness of the material, it is evident that, for this case, a state of near planar axial deformation exists.

Out-of-plane deformation of the textile is illustrated in Figure 6b. The magnitude of the maximum value of this displacement component is approximately 1% of the applied axial value. The length to

thickness ratio of the model is 5.5, producing an average through-thickness Poisson's ratio of υ=0.0 The isosurface shown is at 50%, and once again, the internal displacements are a function of the loc yarn geometry (1). In particular, note that since every point on the isosurface has the same displacemen the regions dominated by the transverse yarns show a greater through-thickness contraction than th regions dominated by axial yarns. This, however, is a local effect, and due to the periodic boundar conditions, must sum to the same through-thickness (y) contraction at every x-z location in the model.

The large non-planar character of the transverse displacements shown in Figure 6c indicates that tl transverse strain in the yarns' fiber direction (near the edges of the RVE) is much less than the strain i the yarn transverse direction (1). Once again, the summation of all of these local phenomenon must equ a common value along the restrained edges for this particular set of boundary conditions.

DISPLACEMENT RESULTS - OUT-OF-PLANE BOUNDARY CONDITIONS

When the upper surface of the RVE is released to deform out of plane, the axial deformation shown Figure 7a results. Unlike what is seen in Figure 3a, there is little effect of lack of out-of-plane constr on the distribution of axial displacement in the model under axial loading (Figure 7a). The c differences are minor and are located near the matrix rich center of the RVE (1).

Out-of-plane deformations are, once again, "dish shaped" and localized (1) as seen in Figure 7b. maximum U_y displacement occurs at (2). This maximum U_y is 69% larger than the correspon displacement for the fully restrained case. Unlike the corresponding thermal load case, where the load is induced in all directions resulting in a somewhat uniform concave surface (Figure 3b), isosurface in Figure 7b is preferential to the axial direction.

When the planar constraint is eliminated completely from the model to simulate a material one RV thick, the axial displacement isosurfaces appear as in Figure 7c. Unlike the more restrained cases, t free-free case has very non-planar isosurfaces of axial displacement indicating that the strain distributi within the model has been significantly altered as a function of weave geometry. Further greatly increas shear strains (1) result. These isosurfaces are somewhat similar to those shown for ΔT in Figure 3c.

The corresponding isosurfaces of out-of-plane displacement are given in Figure 7d. The maximum U is 2400% larger than for the fully restrained case and is very irregular. Here, (1) is at the maximum U while (2) is the minimum for the entire model. The shape of (3), the 50% surface, further illustrates th extreme gradient of displacements in this model. If, for example, this surface is considered the neutr surface, then displacements on either side can be considered to be of opposite sense. While the in-plar requirement for the top and/or bottom surface prevented the large U_y in the constrained models with axi loading, and the force in the transverse yarn counterbalanced much of the force in the axial yarns in th case of thermal loading, no such situation exists in this particular case.

DISPLACEMENT RESULTS - IN-PLANE BOUNDARY CONDITIONS

Unlike the case of uniform temperature change, a free edge in an axially loaded RVE has little effect on the axial displacement. This is seen in Figure 8a.

Figure 8b illustrates the transverse deformation for the one edge free case. The isosurface (1) is the region of maximum transverse displacement (dimpling at the edge). Unlike a laminated material, this dimpling is a function of both the local x- and y-coordinate. Of course, the details are a function of the location of the free edge within the RVE. If, for example, the free surface were at the midplane of this RVE (z=0) the local deformation and strain energy states would likely be very different.

The axial displacement for the limiting case of a structure one RVE wide (both front and back edges released) is shown in Figure 8c. Even with no transverse constraint beyond the boundaries of the representative volume element, and unlike the thermally loaded case, there is little dependence on the transverse (z) coordinate.

The isosurfaces of transverse displacement are shown in Figure 8d. Similar to what is shown in Figure 8b, the transversely compliant region near the center of the RVE has the greatest transverse displacement. The maximum transverse displacement is 500% larger than in the fully restrained case. Once again the x-y dependence is seen, as are angular changes representative of large shear strains (1).

STRAIN ENERGY DENSITY RESULTS

Strain energy density (SED) results for the case of periodic boundary conditions and axial loading are shown in Figure 9a. The yarns contain all of the SED in the model above 2.5 in-lb/in^3. Unlike the case of uniform thermal expansion, the product of axial stress and axial strain dominates the behavior of the material. The maximum value of SED is 11.2 in-lb/in^3 and occurs at the axial yarn centerline between the two constraining transverse yarns. Also, since the transverse yarns are considerably stiffer and take more load than the matrix, the SED in the axial yarns is slightly reduced at the regions of transverse yarn cross-over.

Removal of the out-of-plane constraints produces a SED distribution as shown in Figure 9b. Again the axial yarns dominate the energy distribution in the model; however, both the magnitude and location of the maximum values have changed (1). The maximum value is now 7.2 in-lb/in^3 and is a combined result of axial tension and, recalling the displacements in Figure 7d, local bending.

If both in-plane restraints are removed, a strain energy density distribution similar to that in Figure 9c results. The yarns are once again seen to contain most of the SED. Now the distribution of the maximum values of SED is uniform along the centerline of the axial yarns and little effect of the transverse yarns is noted. The maximum value is 10.6 in-lb/in^3. Comparing this value to that for the fully restrained case (11.2 in-lb/in^3) indicates that transverse constraint contributes only slightly to the maximum value of SED in this material under axial load.

SUMMARY OF RESULTS - MAXIMUMS FOR THERMAL LOADING

Table 3: Thermal Loading

Boundary Condition	U_x (in/F)	U_y(in/F)	U_z(in/F)	SED(in-lb/in^3/F)
Periodic	8.89E-7	16.3E-7	9.19E-7	6.68E-4
Free Top	9.08E-7	21.2E-7	**	**
Free Top / Bottom	9.92E-7	23.9E-7	**	5.06E-4
Free Front	11.5E-7	**	31.6E-7	**
Free Front / Back	10.2E-7	**	47.3E-7	17.9E-4

** not discussed

SUMMARY OF RESULTS - MAXIMUMS FOR AXIAL LOADING

Table 4: Axial Loading

Boundary Condition	U_x (in)	U_y (in)	U_z(in)	SED(in-lb/in^3)
Periodic	0.00275	-2.56E-5	-1.31E-5	11.2
Free Top	0.00275	-4.33E-5	**	**
Free Top / Bottom	0.00275	-61.2E-5	**	7.2
Free Front	0.00275	**	-4.40E-5	**
Free Front / Back	0.00275	**	-6.60E-5	10.6

** not discussed

DISCUSSION OF ANALYSIS

General Comments on the Combined TGM-FEM Analysis

The technique that has been used for this analysis allows:
- Consideration of 3D geometry of textiles
- Interrogation of the details of the behavior of complex textile architectures
- Inclusion of general boundary conditions
- Extraction of components of material response

The method does require:
- Large model size and execution time
- Several simplifications that are unavoidable

Thermal Loading

- The response of even simple textile composites such as plain weaves is fully three-dimensional as shown in the figures in this paper
- Stacking of layers restrains in-plane deformation of the weave
- Severe dimpling is characteristic of an (unrestrained) single layer
- Free edge localizes axial/transverse displacement between transverse yarns
- Low levels of SED for ΔT show similar distribution to mechanical load
- Max SED for fully restrained carbon/epoxy is located in the corners and is dependent on corner geometry
- Decreased mechanical mismatch in glass/epoxy changes location of maximum SED to the transverse yarns (fully restrained case)
- Removing out-of-plane restraint initiates greatest SED away from corners
- Free edge condition redistributes SED into transverse yarns

Mechanical (Axial) Loading

- Although axial deformation is well approximated as two-dimensional, transverse and through-thickness deformation are not
- Unlike the case of thermal loading, axial deformation is not significantly affected by width effects
- The effect of no out of plane constraint is very significant in both deformation and SED response
- Free edge effect is very significant and is a function of both x- and y-coordinate
- Maximum SED is always found in the axial yarns and is altered as a function of the RVE's location within the overall material
- RVE's with little through-thickness constraint are subject to considerable bending

REFERENCES

1. Dexter, H.B., Camponeschi, E.T., and Peebles, L., 3D Composite Materials, NASA CP 24020, Hampton, Va., 1985.

2. Raju, I.S., Foye, R.L., and Avva, V.S., "A Review of Analytical Methods for Fabric and Textile Composites", Proceedings of Indo-US Workshop on Composite Materials for Aerospace Applications, 1990.

3. Carter, W.C., Cox, B.N., Dadkhah, M.S., and Morris, W.L., "An Engineering Model of Woven Composites Based on Mircromechanics," pre-publication.

4. Whitcomb, J.D., "Three-Dimensional Stress Analysis of Plain Weave Composites," NASA TM-101672, Nov. 1989.

5. Woo, K., and Whitcomb, J.D., "Global/Local Finite Element Analysis for Textile Composites," 34th AIAA/ASME/ASCE/AHS/ACS Structures, Structural Dynamics and Materials Conference, pp.

1721-1731, La Jolla, Ca., AIAA-93-1506-CP, 1993.

6. Glaessgen, E.H., Pastore, C.M., Griffin, Jr., O.H., and Birger, A., "Modeling of Textile Composites," Proceedings of the First International Conference on Composites Engineering, New Orleans, 1994.

7. Lene, F. and Paumelle, P., "Micromechanisms of Damage in Woven Composite," Composite Material Technology, PD-Vol 45, ASME, 1992, pp. 97-105.

8. Blacketter, D.M., Walrath, D.E., and Hansen, A.C., "Modeling Damage in a Plain Weave Fabric-Reinforced Composite Material," J. Composites Technology and Research, Vol. 15, No. 2, 1993, pp. 136-142.

9. Pastore, C.M., Gowayed, Y.A., and Cai, Y., "Application of Computer Aided Geometric Modeling for Textile Structural Composites," Computer Aided Design in Composite Material Technology, pp. 45-53, Computational Mechanics Publications, Southampton, UK, 1990.

10. Burr, S.T., private communication, Virginia Polytechnic Institute and State University, Blacksburg, Va, Feb. 1994.

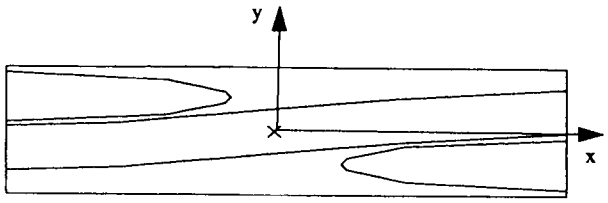

Figure 1a, Side View of RVE

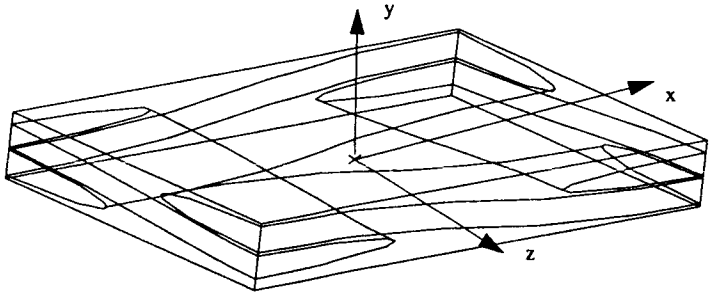

Figure 1b, Isometric View of RVE

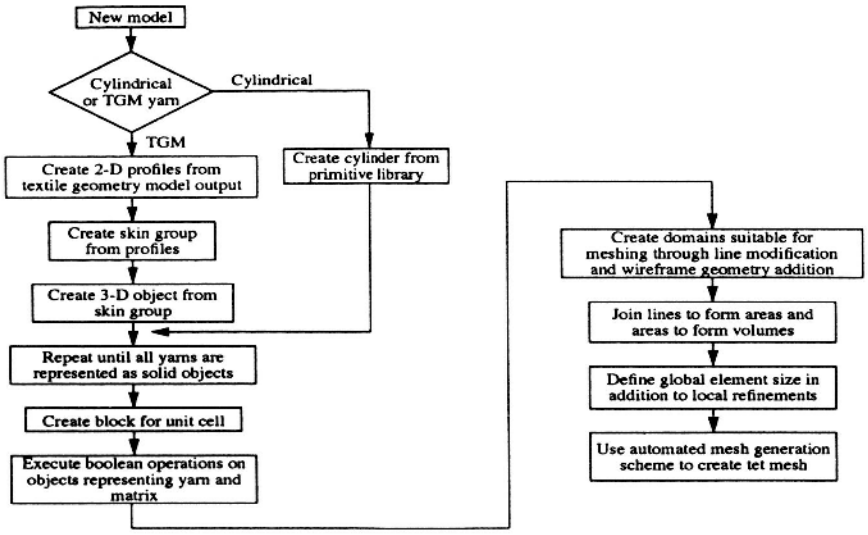

Figure 1c, Model Construction Flowchart

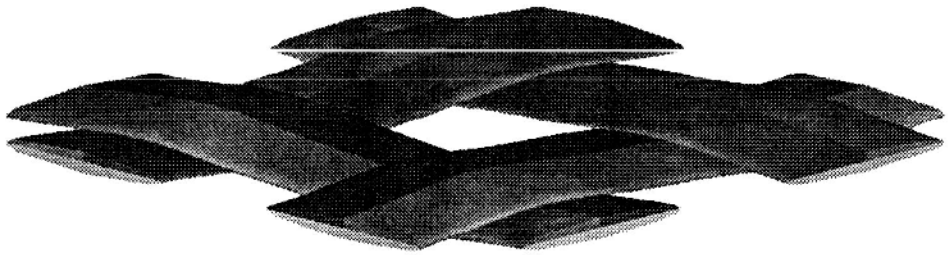

Figure 1d, Yarn Geometry for Plain Weave

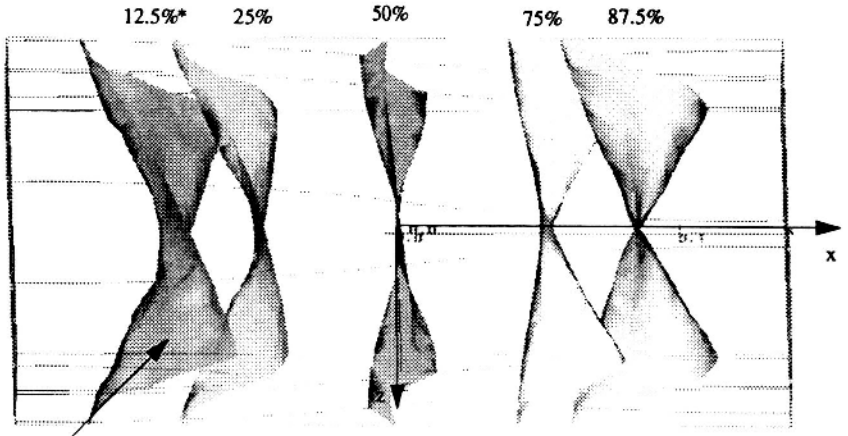

Figure 2a, Axial Displacement, U_x
Periodic Boundary Conditions
$U_{x,\,max}$ = 8.89E-7 in/F

*% of total displacement represented by isosurface

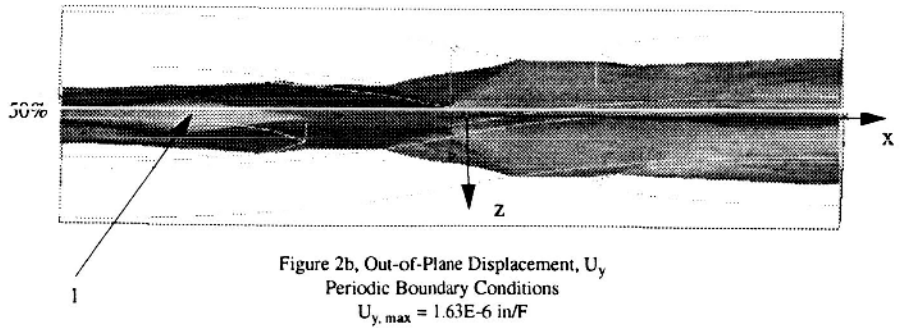

Figure 2b, Out-of-Plane Displacement, U_y
Periodic Boundary Conditions
$U_{y,\,max}$ = 1.63E-6 in/F

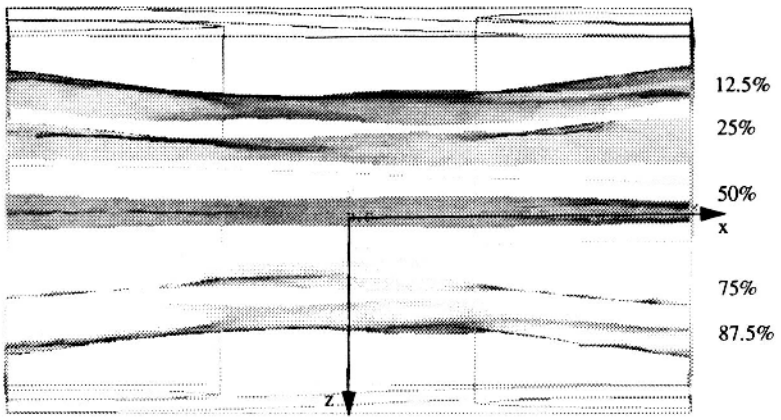

Figure 2c, Transverse Displacement, U_z
Periodic Boundary Conditions
$U_{z,\,max}$ = 9.19E-7 in/F

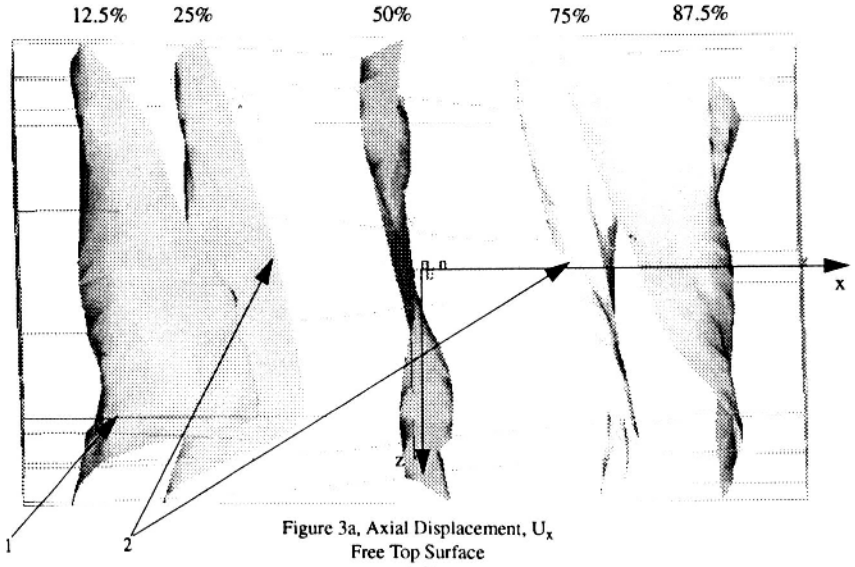

Figure 3a, Axial Displacement, U_x
Free Top Surface
$U_{x,\,max}$ = 9.08E-7 in/F

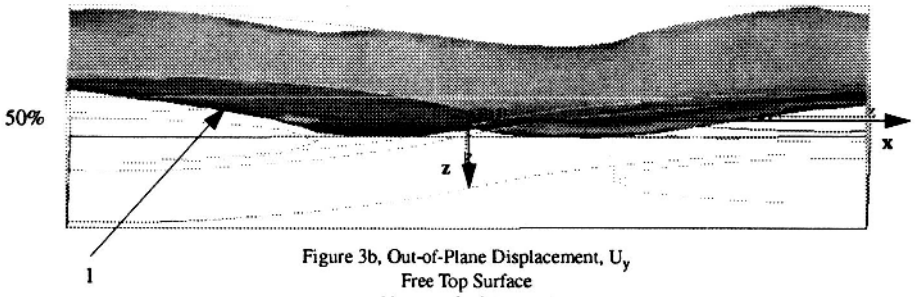

Figure 3b, Out-of-Plane Displacement, U_y
Free Top Surface
$U_{y,\,max}$ = 2.12E-6 in/F

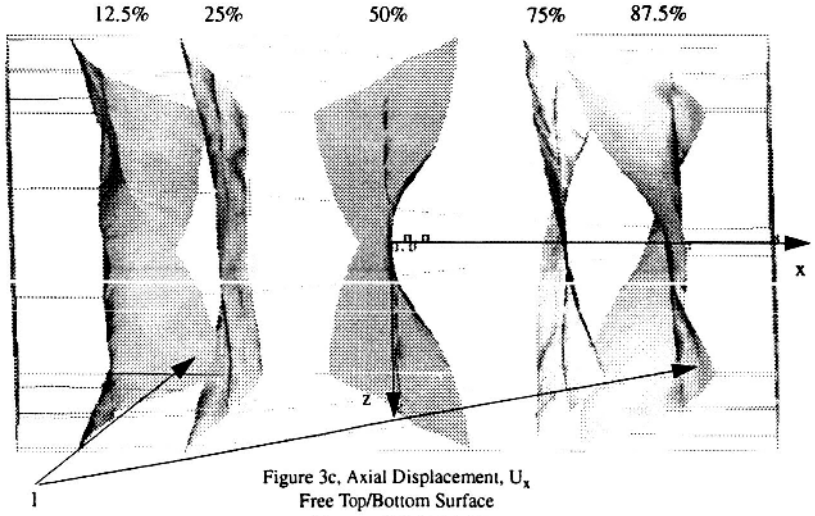

Figure 3c, Axial Displacement, U_x
Free Top/Bottom Surface
$U_{x,\,max}$ = 9.92E-7 in/F

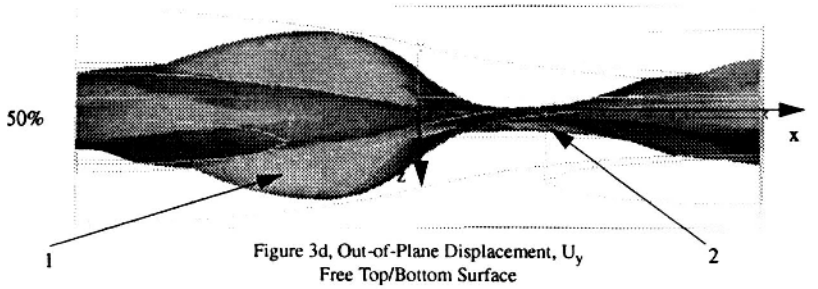

Figure 3d, Out-of-Plane Displacement, U_y
Free Top/Bottom Surface
$U_{y,\,max}$ = 2.39E-6 in/F

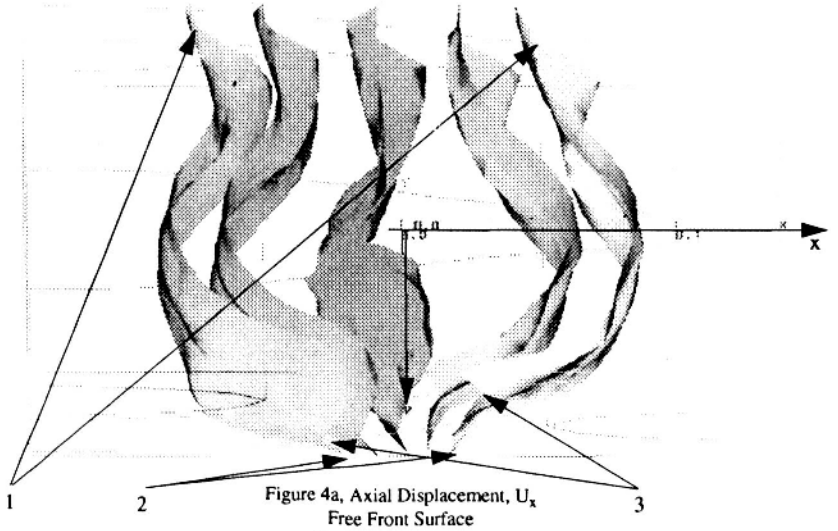

Figure 4a, Axial Displacement, U_x
Free Front Surface
$U_{x,\,max}$ = 1.15E-6 in/F

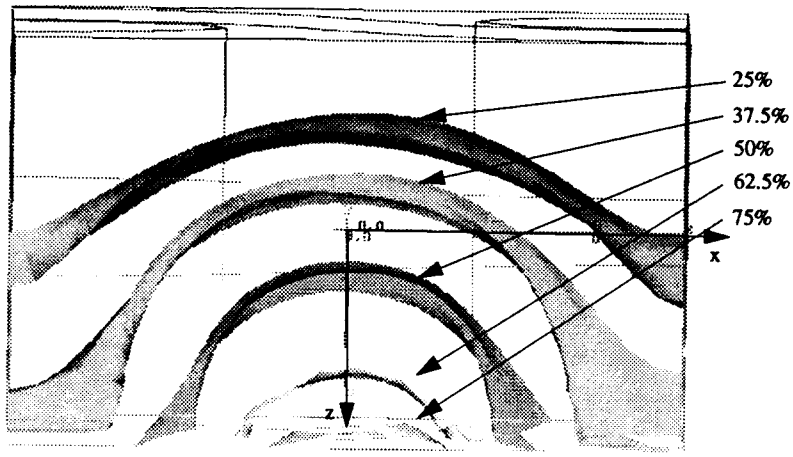

Figure 4b, Transverse Displacement, U_z
Free Front Surface
$U_{z,\,max}$ = 3.16E-6 in/F

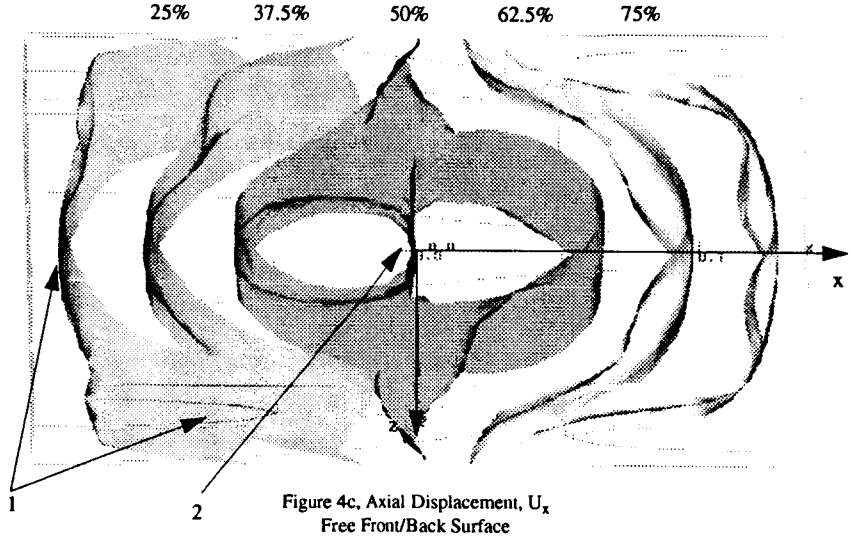

Figure 4c, Axial Displacement, U_x
Free Front/Back Surface
$U_{x,\,max}$ = 1.02E-6 in/F

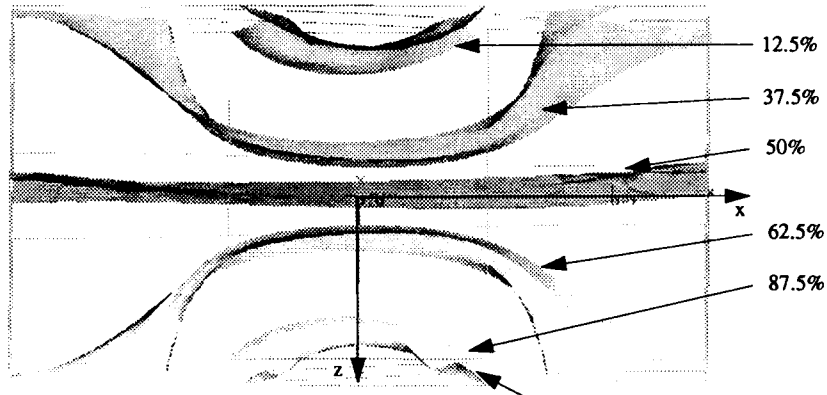

Figure 4d, Transverse Displacement, U_z
Free Front/Back Surface
$U_{z,\ max}$ = 4.73E-6 in/F

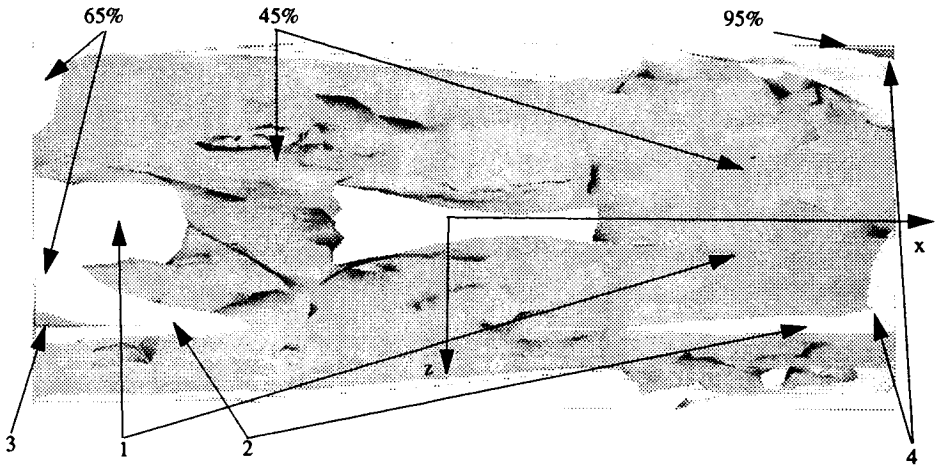

Figure 5a, Strain Energy Density, SED
Periodic Boundary Conditions
0.546E-4<SED<6.68E-4 (in-lb/in^3)/F

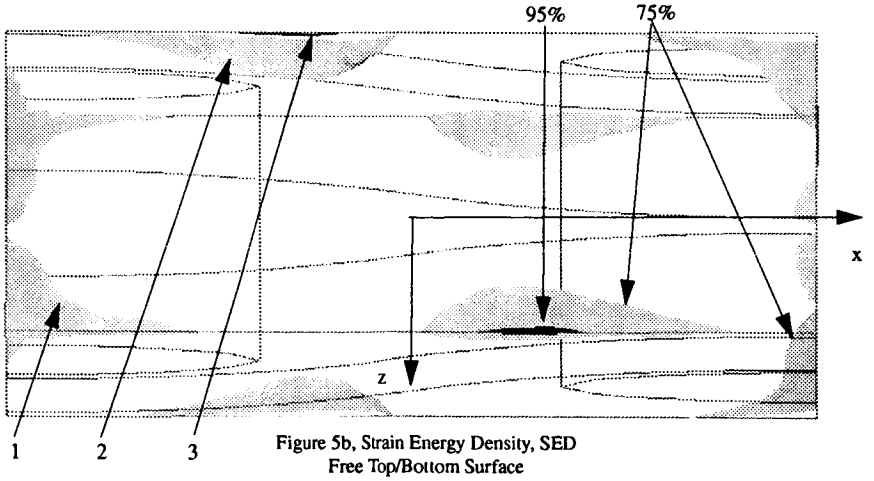

Figure 5b, Strain Energy Density, SED
Free Top/Bottom Surface
0.532E-4<SED<5.06E-4 (in-lb/in^3)/F

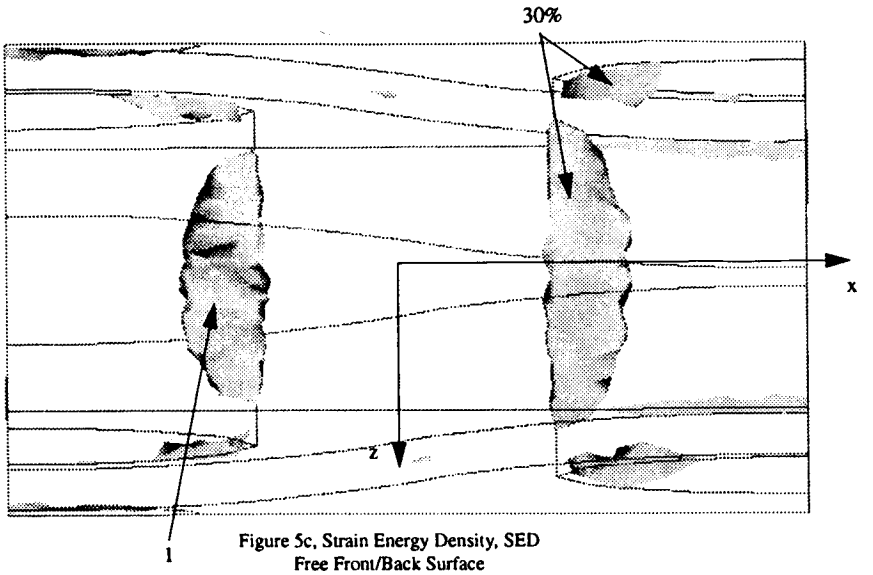

Figure 5c, Strain Energy Density, SED
Free Front/Back Surface
0.248E-4<SED<17.90E-4 (in-lb/in^3)/F

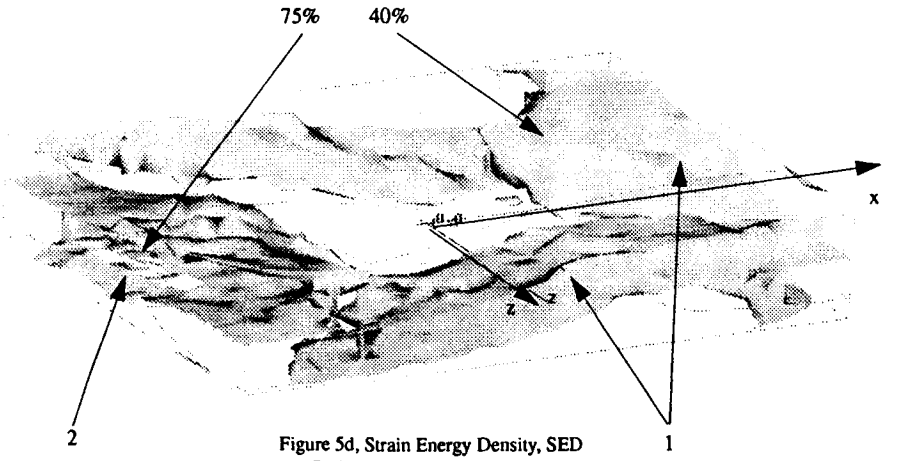

Figure 5d, Strain Energy Density, SED
Periodic Boundary Conditions
Glass/Epoxy Yarns
0.281E-4<SED<4.08E-4 (in-lb/in^3)/F

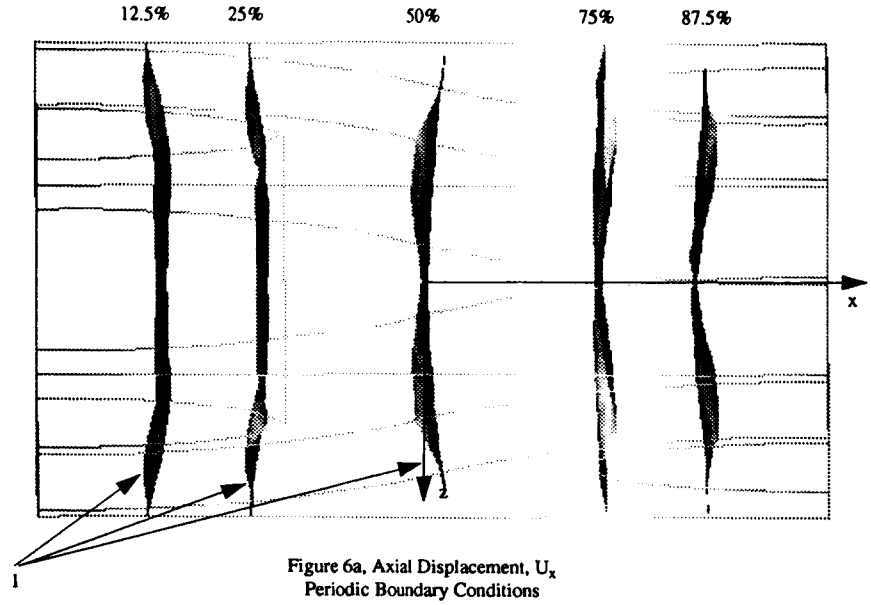

Figure 6a, Axial Displacement, U_x
Periodic Boundary Conditions
$U_{x,\,max}$ = 0.00275 in

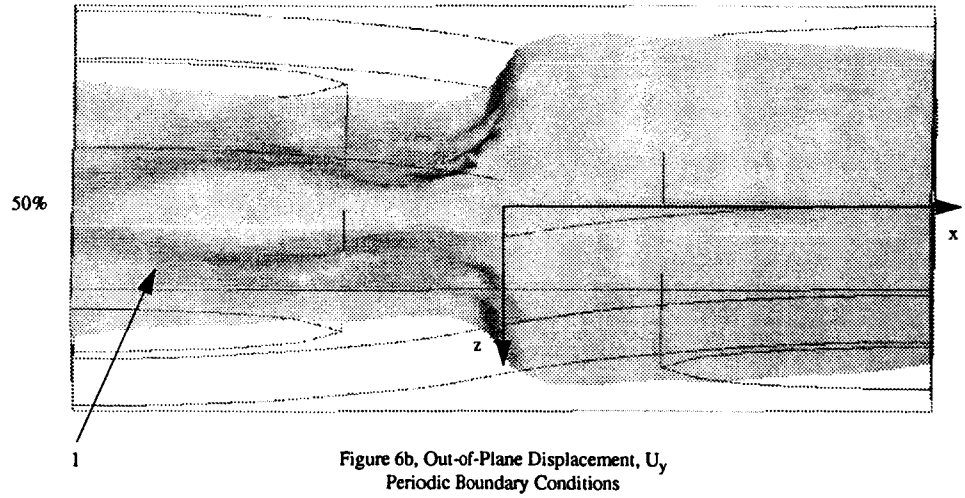

Figure 6b, Out-of-Plane Displacement, U_y
Periodic Boundary Conditions
$U_{y,\,max}$ = -2.56E-5 in

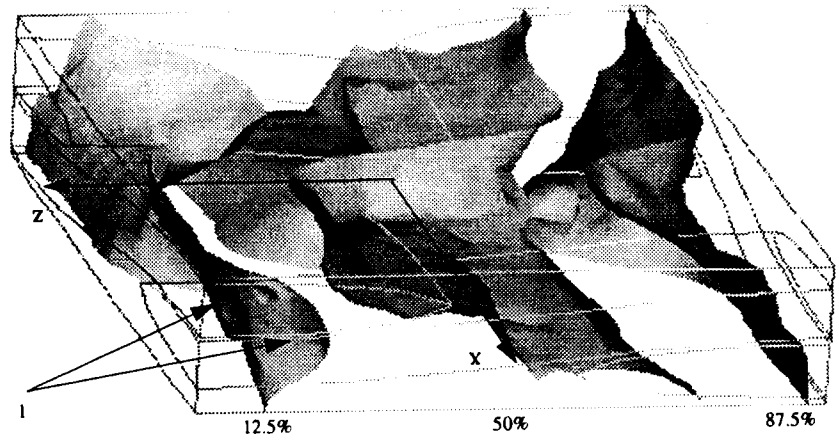

Figure 6c, Transverse Displacement, U_z
Periodic Boundary Conditions
$U_{z,\,max}$ = -1.31E-5 in

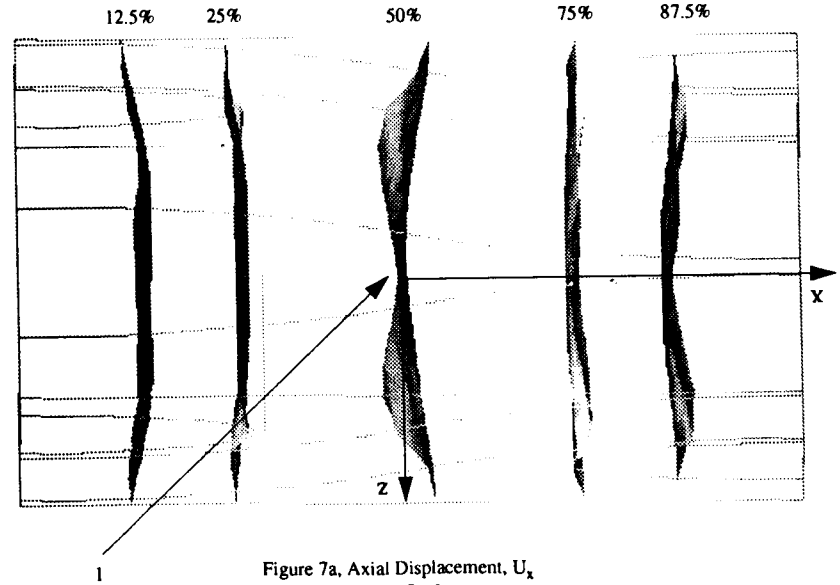

Figure 7a, Axial Displacement, U_x
Free Top Surface
$U_{x,\,max}$ = 0.00275

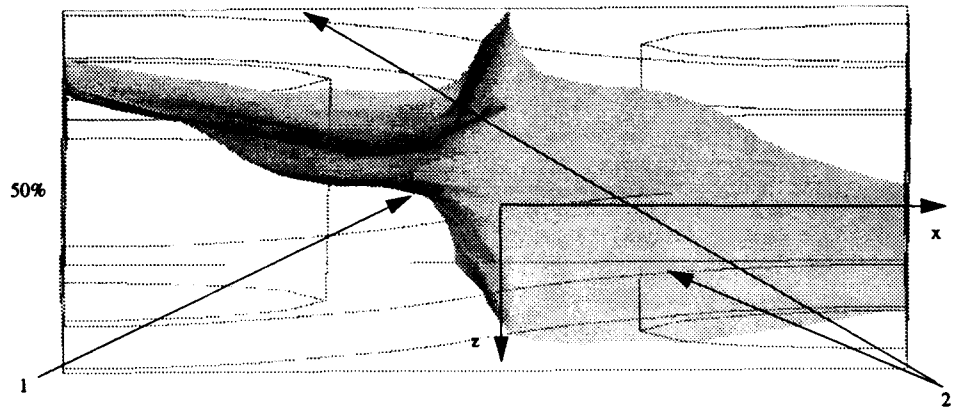

Figure 7b, Out-of-Plane Displacement, U_y
Free Top Surface
$U_{y,\,max}$ = -4.33E-5 in

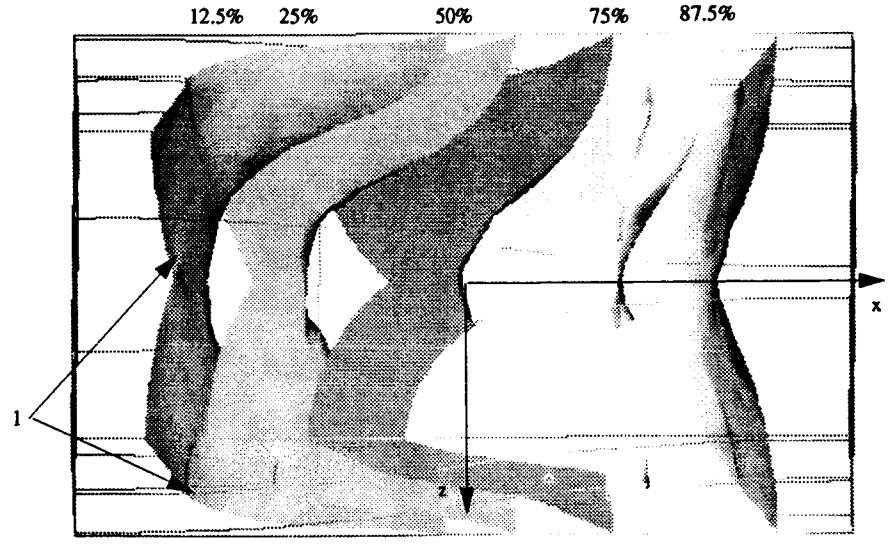

Figure 7c, Axial Displacement, U_x
Free Top/Bottom Surface
$U_{x,\,max}$ = 0.00275 in

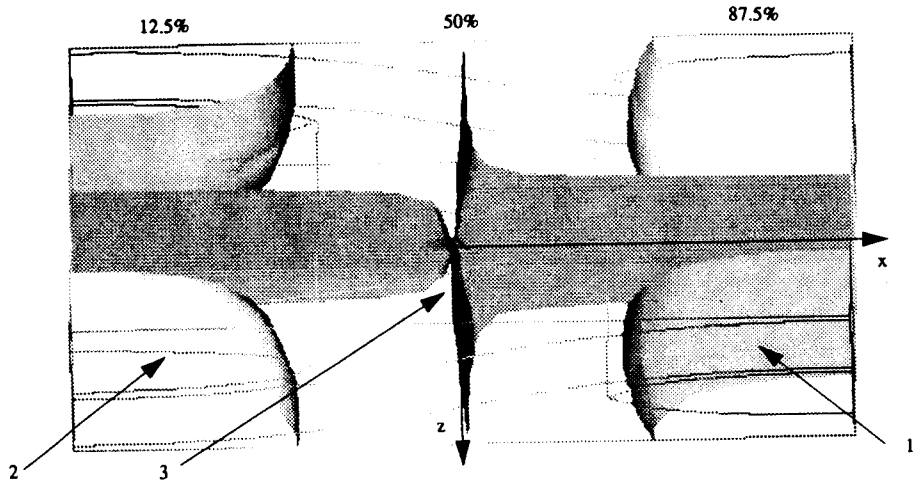

Figure 7d, Out-of-Plane Displacement, U_y
Free Top/Bottom Surface
$U_{y,\,max}$ = -61.2E-5 in

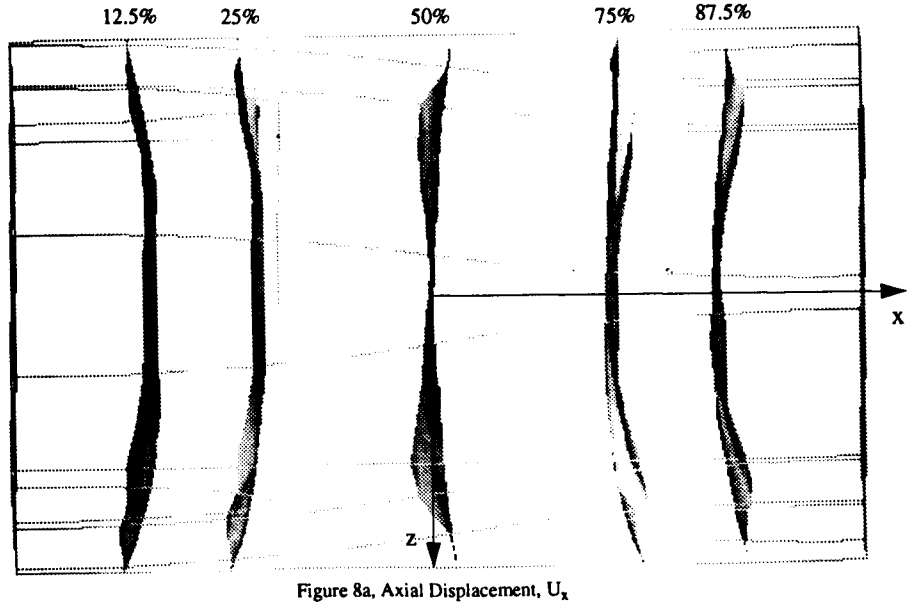

Figure 8a, Axial Displacement, U_x
Free Front Surface
$U_{x,\,max}$ = 0.00275 in

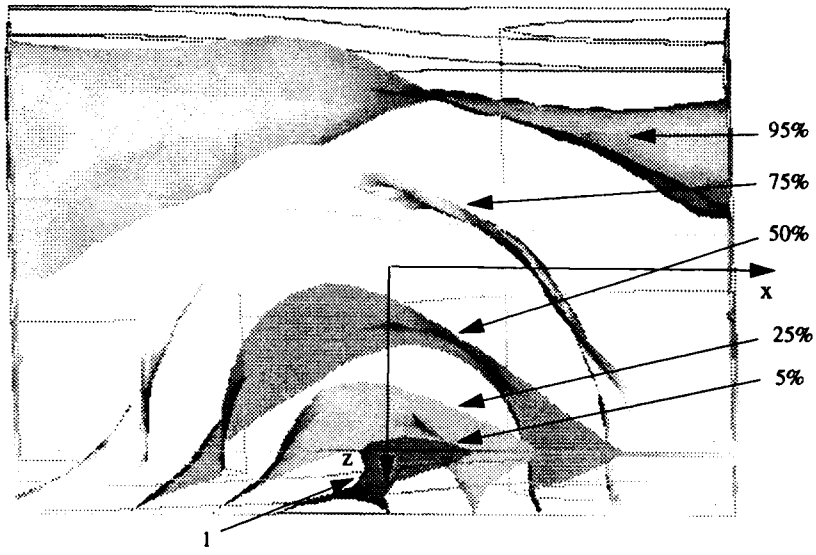

Figure 8b, Transverse Displacement, U_z
Free Front Surface
$U_{z,\,max}$ = -4.40E-5 in

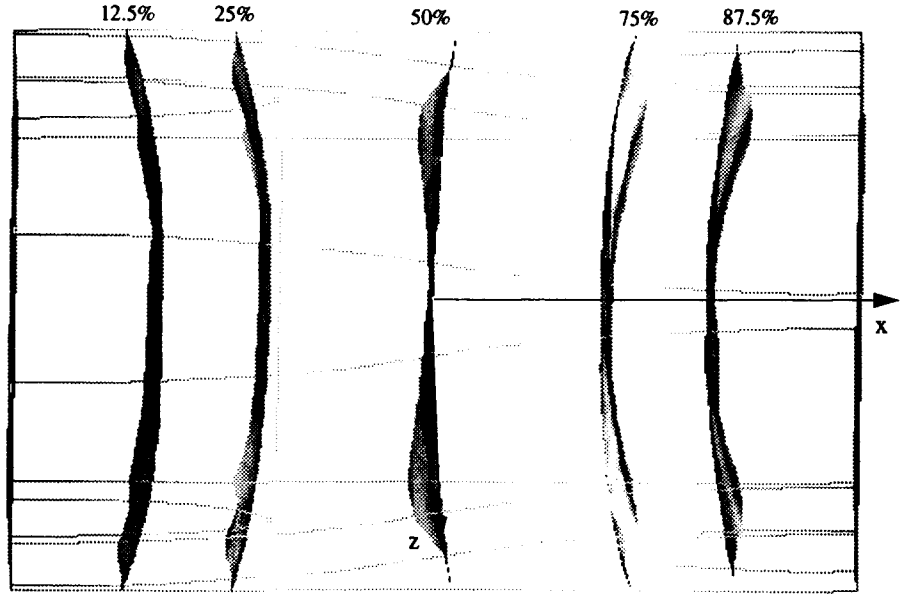

Figure 8c, Axial Displacement, U_x
Free Front/Back Surface
$U_{x,\,max}$ = 0.00275 in

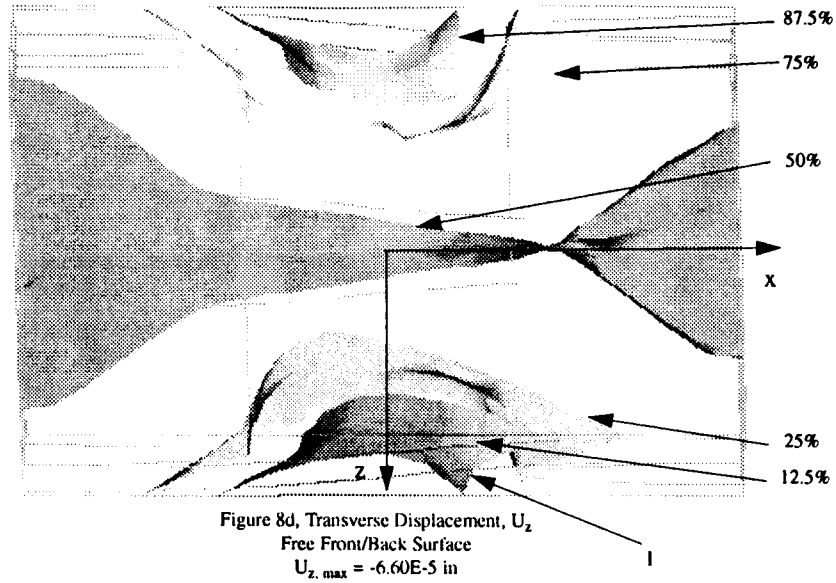

Figure 8d, Transverse Displacement, U_z
Free Front/Back Surface
$U_{z,\,max}$ = -6.60E-5 in

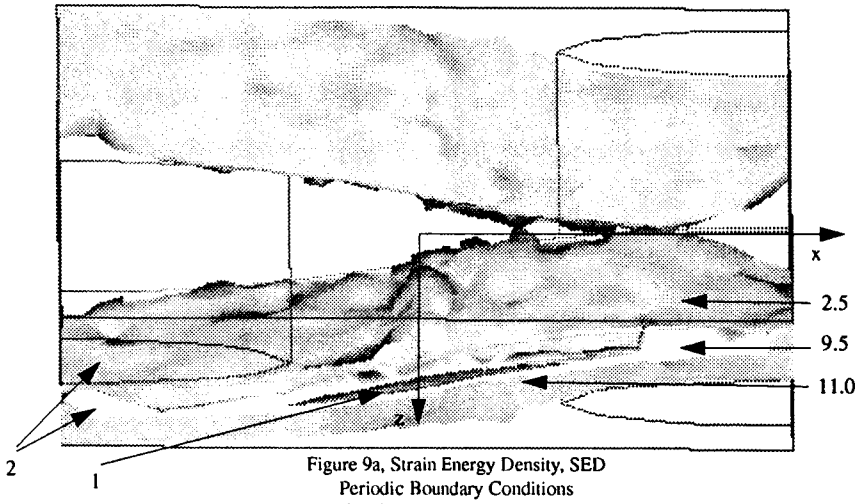

Figure 9a, Strain Energy Density, SED
Periodic Boundary Conditions
0.0035<SED<11.2 in-lb/in^3

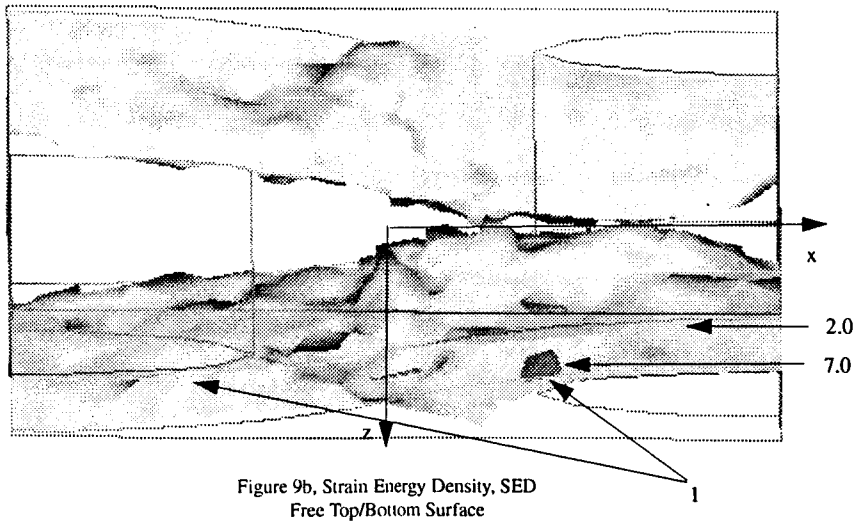

Figure 9b, Strain Energy Density, SED
Free Top/Bottom Surface
0.0545<SED<7.2 in-lb/in^3

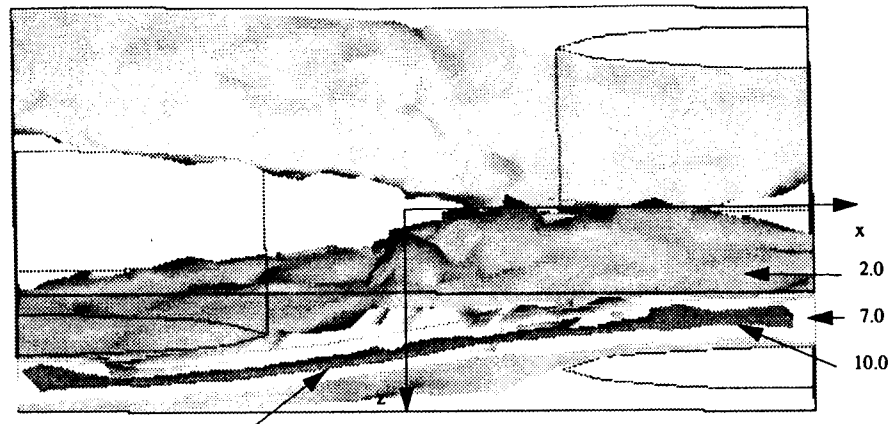

Figure 9c, Strain Energy Density, SED
Free Front/Back Surface
0.0638<SED<10.6 in-lb/in^3